Environmental Science & Technology

Article

Cite This: Environ. Sci. Technol. 2018, 52, 4275−4284

pubs.acs.org/est

Iron Mesh-Based Metal Organic Framework Filter for Efficient Arsenic Removal

Dawei Wang,[†] Stanley E. Gilliland, III,[‡] Xinbei Yi,[†] Kayla Logan,[†] Denver R. Heitger,[§] Heather R. Lucas,[§] and Wei-Ning Wang*[,†]

[†]Department of Mechanical & Nuclear Engineering, [‡]Department of Chemical and Life Science Engineering, and [§]Department of Chemistry, Virginia Commonwealth University, Richmond, Virginia 23219, United States

Supporting Information

ABSTRACT: Efficient oxidation from arsenite [As(III)] to arsenate [As(V)], which is less toxic and more readily to be adsorbed by adsorbents, is important for the remediation of arsenic pollution. In this paper, we report a metal organic framework (MIL-100(Fe)) filter to efficiently remove arsenic from synthetic groundwater. With commercially available iron mesh as a substrate, MIL-100(Fe) is implanted through an in situ growth method. MIL-100(Fe) is able to capture As(III) due to its microporous structure, superior surface area, and ample active sites for As adsorption. This approach increases the localized As concentration around the filter, where Fenton-like reactions are initiated by the Fe^{2+}/Fe^{3+} sites within the MIL-100(Fe) framework to oxidize As(III) to As(V). The mechanism was confirmed by colorimetric detection of H_2O_2, fluorescence, and electron paramagnetic resonance detection of ·OH. With the aid of oxygen bubbling and Joule heating, the removal efficiency of As(III) can be further boosted. The MIL-100(Fe)-based filter also exhibits satisfactory structural stability and recyclability. Notably, the adsorption capacity of the filter can be regenerated satisfactorily. Our results demonstrate the potential of this filter for the efficient remediation of As contamination in groundwater.

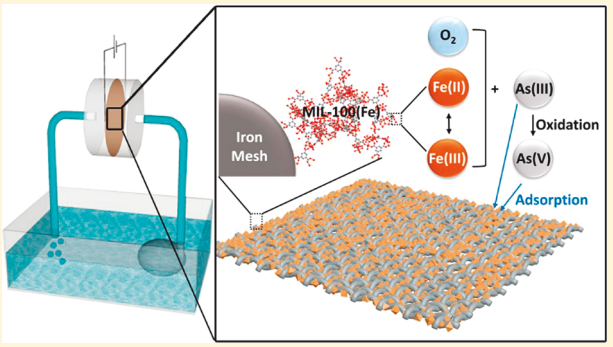

1. INTRODUCTION

Arsenic (As) contamination in groundwater has been threatening human health in some developing countries, where people rely on groundwater as their main supplies for drinking water.[1,2] Even in the United States, people in certain states are suffering from the excessive concentration of arsenic in groundwater.[3] The chronic poisoning by As may cause severe symptoms including skin lesions, hyperkeratosis, and cancer of internal organs, etc.[4] Efficient As mitigating technologies are thus urgently desired. In an earlier review by Mohan and Pittman, different As removal technologies, such as oxidation, coagulation, filtration, and sorption, were compared.[5] Conventional oxidation techniques require careful control of pH.[6,7] For coagulation and its related techniques, the major concern is the production of toxic sludges.[8] The drawbacks of filtration (membrane) techniques are their high running cost and production of toxic wastewater.[9] In contrast, adsorption is evolving as an efficient remediation technique for As removal due to its cost effectiveness and robust operation.[5,10] However, even though negatively charged arsenate [As(V)] can be efficiently removed by adsorption, neutrally charged arsenite [As(III)] with higher toxicity may survive from adsorption.[11] As a result, various synergistic oxidation and adsorption methods have been proposed.[12] Among many candidates, those based on Fenton-like reactions to oxidize As(III) and remove As(V) with the generated adsorbents (e.g., iron oxides) have been proved promising.[13,14] However, even for seriously contaminated groundwater, the highest concentration of As is at the level of $\mu g/L$,[2] which is so low that it cannot facilitate fast reaction kinetics. It is thus expected that by increasing the localized concentration of arsenic around the oxidizing agents, As(III) can be oxidized in a time-efficient way and the generated As(V) will be readily adsorbed. Within this context, a system which is capable of efficiently adsorbing As(III), and thus, increasing its localized concentration will be promising.

Recently, metal organic frameworks (MOFs) have attracted intensive attention due to their superior surface areas and nanoscale pore sizes and have shown significant capacity for gas adsorption.[15,16] MOFs have also found their applications in the adsorption of aqueous contaminants, such as dyes and metal ions.[17,18] Several recent studies have demonstrated the promising feature of MOFs and/or their composites for efficient As removal.[19−25] For example, UIO-66, ZIF-8, and Fe-BTC have been used as powder adsorbents for As removal.[20,22−24] The magnetic composites can help to recycle materials.[19,25] The MnO_2-ZIF-8 composite powders have shown that the oxidation of As(III) into As(V) is helpful for

Received: December 2, 2017
Revised: March 6, 2018
Accepted: March 7, 2018
Published: March 7, 2018

DOI: 10.1021/acs.est.7b06212
Environ. Sci. Technol. 2018, 52, 4275−4284

a faster removal of arsenic.[21] However, these attempts have raised two critical issues for practical use. (1) Better recycle approaches. As many environmental functional materials which are used as dispersion, the above-reported adsorbents are in powder form. The recycle of these particulate adsorbents remains a major concern for groundwater safety. Secondary contamination may occur if these particulate adsorbents are not removed from the water body. (2) Simultaneous adsorption and oxidation. Solo adsorption approach cannot completely solve the As issue as the more toxic As(III) still remains inside the adsorbents, which require additional treatments. Thus, a MOFs-based system which can address these issues will be promising for efficient control of As contamination in groundwater via simultaneous adsorption and oxidation.

Within this context, we hereby demonstrate an iron mesh-based MOFs filter for efficient removal of As. The iron mesh serves as an substrate and provides iron ions for the in situ growth of an iron-based MOF (MIL-100(Fe), MIL represents Materials of Institut Lavoisier).[16] MIL-100(Fe) is capable of increasing the localized concentration of As around the filter due to its mesoporous structure, high surface area, and ample surface sites.[19] As a result, the coordinatively unsaturated iron sites[26] within the MIL-100(Fe) initiate the Fenton-like reactions to oxidize As(III) to As(V) rapidly with the aid of external voltage and air, while the generated As(V) is adsorbed by MIL-100(Fe) (Scheme 1).

Scheme 1. (Left) Set-up of the Iron Mesh-Based Filter for Arsenic Removal; (Right) Proposed Mechanism of the Efficient Arsenic Removal of This System[a]

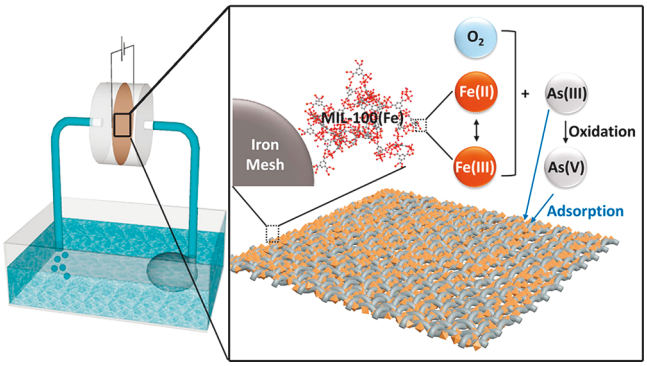

[a]The ball and stick structure in the right figure represents MIL-100(Fe).

2. MATERIALS AND METHODS

2.1. Chemicals and Materials. Sodium arsenite ($NaAsO_2$, ≥90%), sodium arsenate dibasic heptahydrate ($Na_2HAsO_4 \cdot 7H_2O$, ≥ 98%), calcium chloride ($CaCl_2$, ≥96%), magnesium chloride ($MgCl_2$, ≥98%), sodium metasilicate (Na_2SiO_3, ≥98%), sodium bicarbonate ($NaHCO_3$, ≥99.7%), sodium phosphate (NaH_2PO_4, 96%), and trimesic acid (H_3BTC, 98%) were purchased from Sigma-Aldrich. Coumarin ($C_9H_6O_2$, 98%) was received from Fisher Scientific. Steel woven wire cloth (60 × 60 mesh, diameter of single iron wire = 0.19 mm) was obtained from McMaster-Carr (U.S.A). Ultrapure water (18.2 MΩ·cm, produced by Barnstead SMART2PURE system, ThermoFisher Scientific) was used throughout the experiments.

2.2. Synthesis of MIL-100(Fe) on Steel Woven Wire Cloth. In a typical synthesis, 0.01 g of H_3BTC and 9.56 mL of H_2O were mixed by sonication. Then a steel woven wire cloth (rinsed with methanol three times to remove impurities) and the above mixed solution were introduced into a microwave reactor and allowed to be heated at 140 °C for 30 min. After cooling down to room temperature, the product was collected and washed with water (80 °C, 3 h) to remove unreacted chemicals. The product was further dried in an oven (80 °C, overnight) for characterization and use.

2.3. Batch Experiments. Synthetic Bangladesh groundwater, which contained 8.2 mM $NaHCO_3$, 2.5 mM $CaCl_2$,1.6 mM $MgCl_2$, 0.025 mM NaH_2PO_4, and 0.246 mM Na_2SiO_3, was used.[12] Either $NaAsO_2$ or $Na_2HAsO_4 \cdot 7H_2O$ was used as As source (500 μg/L). The pH value of the synthetic groundwater was 8.57, and the electrical conductivity was 1415 μS/cm. The effect of dissolved organic matter (DOM) on the filtration performance was studied by spiking a certain amount of humic acid (HA, from Sigma-Aldrich, 0.25, 2.5, and 25 mg/L for HA) into the synthetic Bangladesh groundwater. These concentrations of HA are broad enough since the average concentration of DOM in Bangladesh is 2.5 mg/L.[27] In a typical experiment, 1.5 L of synthetic water in a tank was circulated through the filter with a submersible pump (HG16, flow rate = 100 L/h). Air was purged (flow rate = 20 mL/min) into the tank to increase the concentration of dissolved oxygen. A direct-current power supply system (OMRON S8VM-01505C) was used to provide voltage to the steel mesh (as shown in the Scheme 1). During the experiments, water samples were collected with syringe filters (0.45 μm Nylon membrane, VWR) at specific time intervals (every 30 min in the first 2 h and every 1 h in the subsequent 4 h). To determine the adsorption capacity of the filter, As(III)- or As(V)-dosed water (concentration varied from 0.5 to 30 mg/L) was fed through the filter at room temperature and water samples were collected at 6 h to measure As concentration. Characterization and measurements methods are detailed in the Supporting Information.

3. RESULTS AND DISCUSSION

3.1. Fabrication of MIL-100(Fe)-Based Filter. Commercially available steel woven wire cloth (denoted as iron mesh below) was used as the iron source for the in situ growth of MIL-100(Fe). After hydrothermal treatment in the solution of H_3BTC, orange crystals are formed on the iron mesh (Figure 1A and 1B). As shown in the optical microscopy images, the surface of the pristine iron wires is smooth and shiny (Figure 1C and 1D). After the growth of MIL-100(Fe), a significant increase in wire diameter is observed (Figure 1E). Closer observation indicates that the orange crystals with specific morphologies distribute on the iron mesh (Figure 1F). The morphological change of the iron mesh before and after MIL-100(Fe) growth is also apparent from the corresponding scanning electron microscopy (SEM) images (Figure S1). It should be noted that the coverage of the crystals on the iron mesh is uniform and complete. For the filter application, the iron meshes were cast into circles with a diameter of 25 mm for the growth of MIL-100(Fe) (Figure 1G). It is also expected that this fabrication procedure could be readily scaled up with larger iron meshes and reaction containers.

To verify the composition, morphology, and porous structure of the orange crystals, X-ray diffraction (XRD), transmission electron microscopy (TEM), and nitrogen sorption analysis

DOI: 10.1021/acs.est.7b06212
Environ. Sci. Technol. 2018, 52, 4275−4284

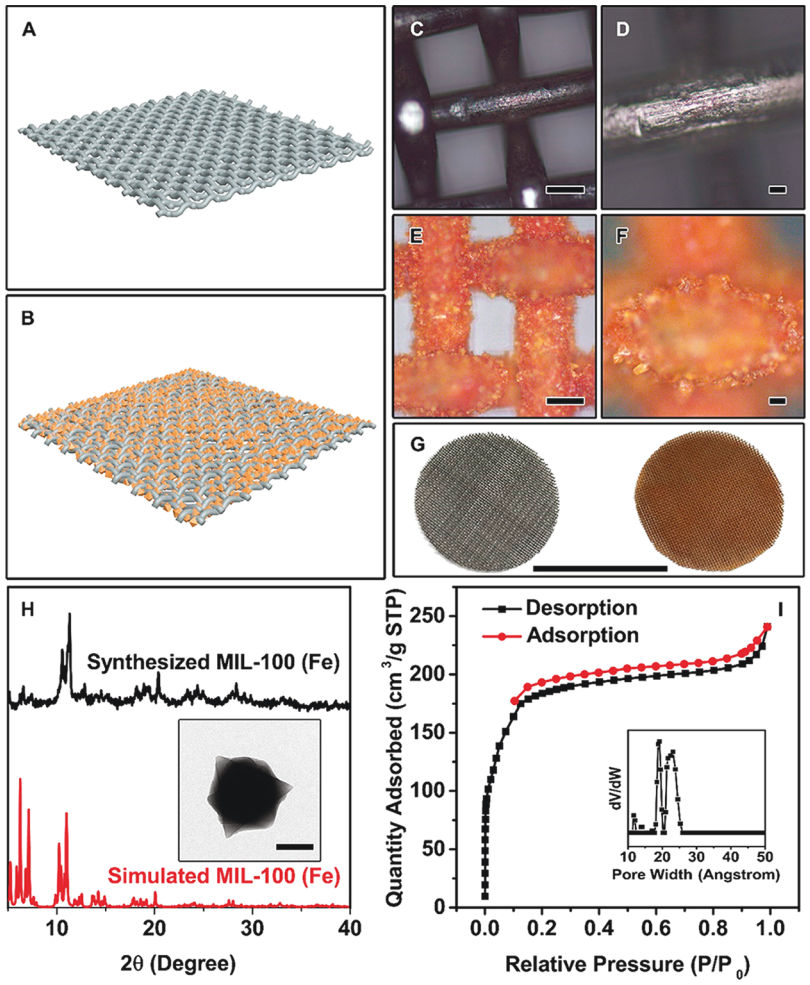

Figure 1. Schematic illustration of (A) pristine iron mesh- and (B) MIL-100(Fe)-based filter. (C and D) Optical microscopy images of pristine iron mesh. (E and F) Optical microscopy images of MIL-100(Fe)-based filter. (G) Digital image of the circle iron mesh before (left) and after the growth of MIL-100(Fe) (right). (H) XRD pattern of the synthesized MIL-100(Fe) crystals; (inset) TEM image; scale bar represents 500 nm. (I) N_2 sorption isotherms; (inset) pore size distribution plot. Scale bars in C−F represent 200 μm. Scale bar in G represents 25 mm.

were carried out, respectively. The XRD pattern of the crystals scratched off from the iron mesh indicates the successful synthesis of MIL-100(Fe) (Figure 1H).[26] The corresponding TEM image also shows that the orange crystal is made up of octahedral crystals, which is the typical shape of MIL-100(Fe) (inset of Figure 1H). The nitrogen sorption of the product displays type I isotherms, suggesting its microporosity.[28] Meanwhile, the BET surface area of the synthesized MIL-100(Fe) was measured to be ~720 m^2/g, which is significantly more than that of pristine iron mesh (~0.25 m^2/g, Supporting Information). MIL-100(Fe) also has two major pore sizes of around 2 nm (inset in Figure 1I), which are large enough for arsenic ions to diffuse inward. It is noteworthy that MIL-100(Fe) connects with the iron mesh through covalent bonds,[29] which are strong enough to maintain a satisfactory stability (as discussed in the following section). The detailed formation mechanism of this filter is discussed in the Supporting Information.

3.2. Removal of Arsenic. Experiments were conducted with mimic Bangladesh groundwater, as detailed in the Materials and Methods. Different filters were sealed into a filter holder (Figure S2), where water flows through. All of the experimental parameters are listed in Table S1. As shown in Figure 2A, even for pristine iron mesh, the removal of both As(III) and As(V) was observed. Specifically, nearly 17% of As(V) and 10% of As(III) were removed after the 6 h filtration with pristine iron mesh as filters, respectively. Some studies have reported that iron oxides and iron salts have a satisfactory adsorption performance toward arsenic.[13,30−32] Meanwhile, it has been recognized that a higher concentration of sodium and water hardness accelerate the corrosion of iron,[33] which produces both iron salts and iron oxides.[34] As a result, the adsorption of arsenic over the pristine iron mesh may be attributed to the adsorption capacity of iron salts or iron oxides produced because of the corrosion of iron. This will be discussed in detail in the next section.

Notably, a rapid removal of arsenic over MIL-100(Fe)-based filters was recorded. Under certain conditions, as listed in Table S1, a satisfactory performance which meets the safety limit for drinking water (i.e., 10 μg/L, recommended by WHO)[5] was achieved. For example, almost 90% of As(III) and all As(V) was removed after 6 h with MIL-100(Fe)-based filters (Figure 2A and Table S1). Regardless of the types of the filters, a higher removal efficiency of As(V) was always observed than that of As(III), which is consistent with the studies on the arsenic removal with adsorption.[5,19] This is because As(V) usually exists as forms with negative charges, which can be efficiently

DOI: 10.1021/acs.est.7b06212
Environ. Sci. Technol. 2018, 52, 4275−4284

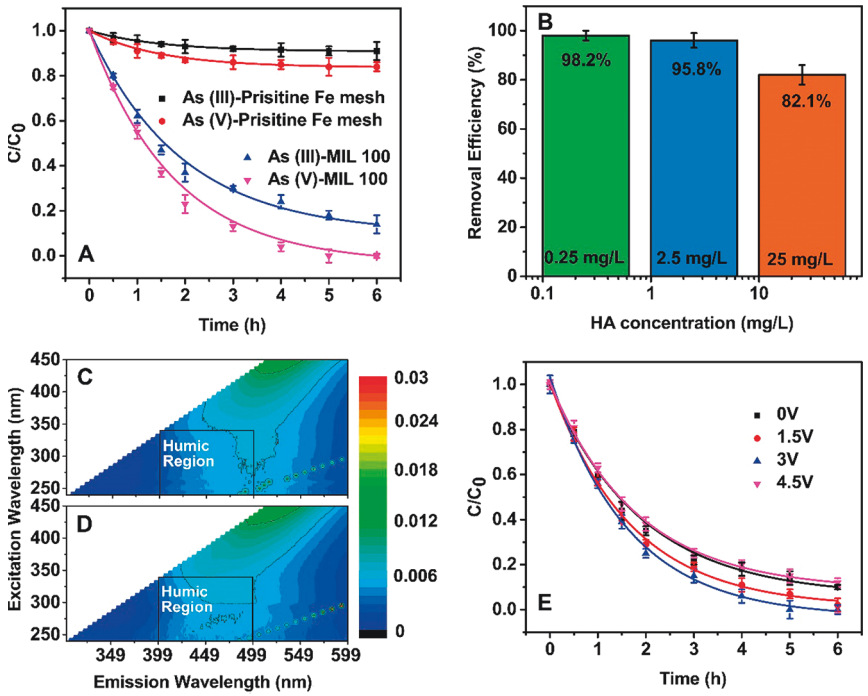

Figure 2. Removal of arsenic under different conditions: (A) solo adsorption of As(III) and As(V). (B) Effect of HA with different concentrations on the removal efficiency (condition 3 V and air bubbling). (C and D) EEMs of the synthetic Bangladesh groundwater (in Raman units) spiked with HA (2.5 mg/L) before and after treatment, respectively. (E) As(III) removal with simultaneous air bubbling and voltage applying.

removed by adsorption, while As(III) may survive from the adsorption process since it is usually neutrally charged.[11]

We also found that the removal kinetics of arsenic over different filters fit well with a pseudo-first-order model, which is consistent with a recent study[35]

$$C_t = C_e + (C_0 - C_e)e^{-kt} \quad (1)$$

where C_t is the concentration of total arsenic (unit μg/L) at time t (unit hour), C_e is the equilibrium concentration of arsenic (unit μg/L), C_0 is the initial concentration of arsenic (500 μg/L), while k represents the first-order rate constant (unit h^{-1}). All of the calculated parameters of the model are summarized in Table S1. The fitted removal kinetics are plotted as curves in Figure 2A. The pH of the groundwater was increased by 0.15 after 6 h (conditions air bubbling and 3 V voltage), probably due to the escape of dissolved CO_2.[32]

In addition, HA as a representative DOM, which is an important component in groundwater, was spiked into the synthetic Bangladesh groundwater to investigate its effects on the filtration performance. As shown in Figure 2B, although negative effects of HA on the As removal efficiency were observed, which are consistent with previous studies,[36−38] the MIL filter fabricated in this study still demonstrated a satisfactory performance. For example, even with HA of 2.5 mL/g (average concentration in groundwater), the total As removal efficiency of the filter is still as high as 95.8% (Figure 2B). However, a higher concentration of HA can reduce the removal efficiency, which may be due to the competitive sorption between DOM and As species on the MIL filter.[36] Competitive oxidation between As(III) and DOM could be another reason. As shown in Figure 2C and 2D, a blue shift of the excitation/emission in the humic region within the fluorescence excitation emission matrices (EEMs) was observed, indicating that decomposition of condensed moieties of HA into smaller molecules.[39] The decomposition of DOM by the oxidants produced in the system (Figure S3) suggested that less As(III) was oxidized into As(V). Another possible As sorption inhibitor, the complexes of As−Fe−DOM, which were frequently found in other research,[40−42] was less likely responsible in our study, since no such complexes were observed in the synthetic groundwater even after 6 h operation (Figure S4). The absence of the complexes also confirmed the stability of the MIL-100(Fe) filter (Figure S4). The absence of complexes of As−DOM (Figure S5) further confirmed that the negative effects from HA were mainly attributed to its competitive sorption and oxidation with As on the filter.

We also investigated the effect of the increased concentration of dissolved oxygen on the removal efficiency of As by bubbling air into the water tank. As shown in Table S1, no obvious change was observed for the removal kinetics of As(III) over pristine iron mesh filter when air is bubbled in the feed tank. For example, the equilibrium concentrations of As(III) over pristine iron mesh for with and without air bubbling are 454.35 and 454.7 μg/L, respectively. However, for the MIL-100(Fe)-based filter, the equilibrium concentrations with and without air bubbling are 42.6 and 68.5 μg/L, respectively, indicating a more extensive removal of As(III) for MIL-100(Fe)-based filter when the concentration of dissolved oxygen is high. Since the adsorption rate of As(V) is faster than that of As(III), a possible oxidation from As(III) to As(V) may happen when air is introduced into this system. This oxidation under air bubbling condition may be ascribed to the ability of the Fe^{2+}/Fe^{3+} couple to activate oxygen to produce oxidants (eqs 2−4)[30]

$$Fe^{2+} + O_2 \rightarrow O_2^{\cdot -} + Fe^{3+} \quad (2)$$

$$Fe^{2+} + O_2^{\cdot -} + 2H^+ \rightarrow Fe^{3+} + H_2O_2 \quad (3)$$

$$Fe^{2+} + HO_2^{\cdot} + H^+ \rightarrow Fe^{3+} + H_2O_2 \quad (4)$$

DOI: 10.1021/acs.est.7b06212
Environ. Sci. Technol. 2018, 52, 4275−4284

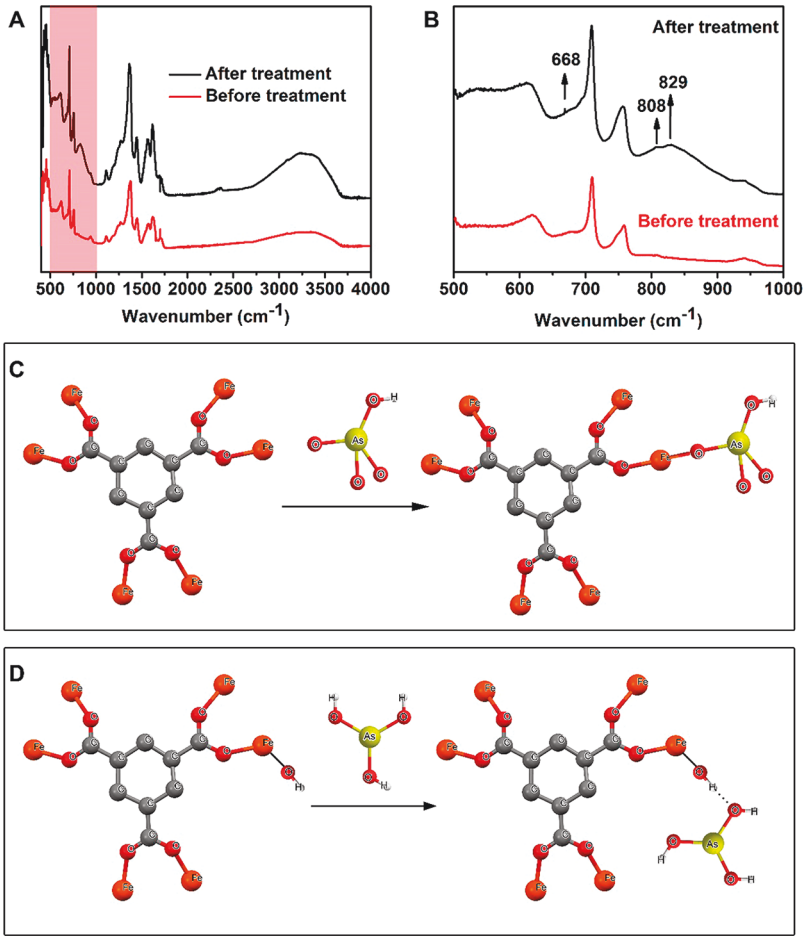

Figure 3. (A and B) FTIR spectra of the MIL-100(Fe) before and after treatment. (C) Proposed As(V) and (D) As(III) adsorption mechanisms over MIL-100(Fe) under pH 8.57.

Notably, when certain voltages were further applied, the removal efficiency of As(III) changed significantly. For example, when the applied voltage was increased from 0 to 1.5 V (Figure 2E), the removal efficiency of As(III) increased from 91.5% to 94.7% (Table S1). When the voltage was further increased to 3 V (Figure 2E), 100% of As(III) can be removed within 6 h. However, a higher voltage input (4.5 V, Figure 2E) decreased the As(III) removal efficiency to 90.9%. The advantages of using relative low voltages can be ascribed to the Joule heating effect which further improves the oxidation rate of As(III) since the temperature increase generally results in the enhancement of reaction kinetic constants. However, the generated Joule heating could also decrease the removal efficiency of As(III) since a higher temperature usually decreases the adsorption rate according to the Arrhenius equation.[28] As a result, it can be concluded that the balance between the oxidation rate and the adsorption capacity due to the Joule heating determines the removal efficiency of As(III).

The Joule heating introduced by the applied voltage was further verified by the temperature changes when different voltages were applied. According to the Joule's first law, the power of heating (P) generated by an electrical conductor is proportional to the square of the applied voltages (V)

$$P \propto V^2/R \tag{5}$$

where R is the electrical resistance of the conductor, which is assumed to be constant. It should be noted that the heat is mainly generated by the iron wire wrapped inside the filter since MIL-100(Fe) is not conductive (electrical resistance > 2000 kΩ). The ambient environment could be further heated through thermal convection and radiation. Thus, we observed that the temperature of the surface of MIL-100(Fe)-based filter increased with the increasing voltages. Without applying voltages, the temperature of the filter surface is 23.2 °C, the same as water under ambient condition. When the voltage was increased, the surface temperature of the filter was also increased (24.8 °C for 1.5 V, 27.0 °C for 3.0 V, and 29.8 °C for 4.5 V). The negative effect of Joule heating on adsorption was further verified by another control experiment. When no air was bubbled into the system and only voltage was applied, a continuous decrease of As(III) removal efficiency was observed with the increase of applied voltage (Figure S6 and Table S1).

3.3. Mechanism Investigation. The species distribution of arsenic under different pH values was plotted using Visual MINTEQ (Figure S7). The results suggested that the predominant species for As(III) is H_3AsO_3 and that for As(V) is $HAsO_4^{2-}$ under the experimental pH of 8.57. To understand how MIL-100(Fe) helps concentrate arsenic, FTIR analysis was conducted. As shown in the full-scan spectra (Figure 3A), some changes were observed in the range from 500 to 1000 cm^{-1} after the filter was used for As removal. Closer observation indicated three bands at 668, 808, and 829 cm^{-1} evolved (Figure 3B). The band at 668 cm^{-1} is indexed to As−OH asymmetric stretching.[24] The two bands at 808 and

DOI: 10.1021/acs.est.7b06212
Environ. Sci. Technol. 2018, 52, 4275−4284

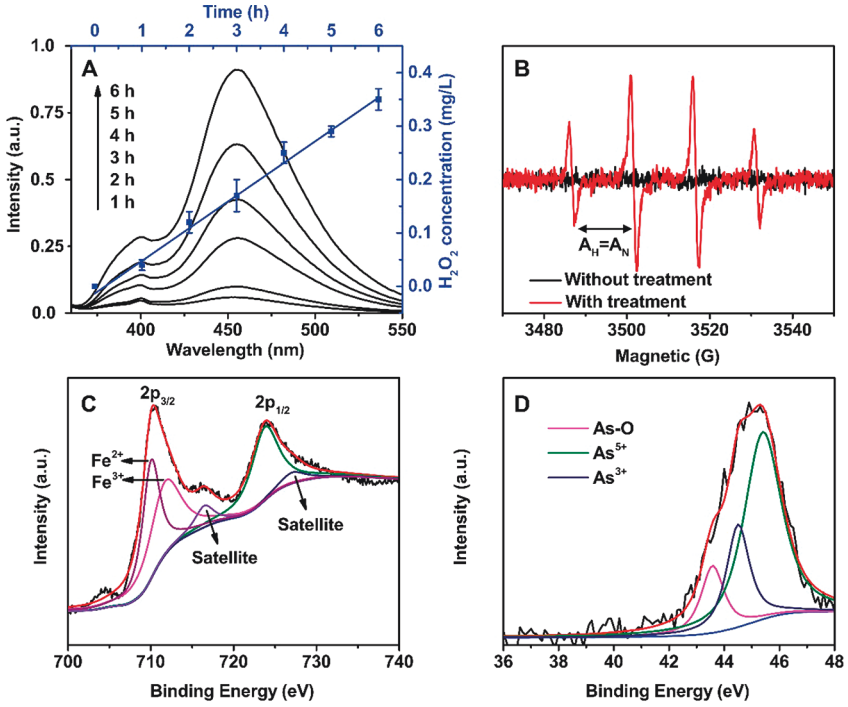

Figure 4. (A) Production of H_2O_2 in the filter (3 V with air bubbling, blue plot) and evolution of fluorescence spectra with time (black curves). (B) EPR spectra of DMPO-treated samples without (0 h) and with treatment (2 h) by the MIL-100(Fe) filter. (C) XPS spectrum of Fe 2p from MIL-100(Fe) before use. (D) XPS spectrum of As 3d from MIL-100(Fe) after use.

829 cm^{-1} are considered as the "splitting" of the υ(As−O) vibration, which are assigned to Fe−O−As groups and nonsurface-complexed As−O bonds, respectively.[43] These two vibrations also correspond to the symmetric and asymmetric stretching modes of $AsO_3(OH)^{2-}$ complex.[43,44] As a result, a possible adsorption mechanism is that $HAsO_4^{2-}$ binds to the coordinatively unsaturated iron sites within MIL-100(Fe), forming $AsO_3(OH)^{2-}$ complex and Fe−O−As bonds (Figure 3C). However, we did not observe the band of As(III) (~800 cm^{-1}), consistent with two previous studies.[43,44] The absence of the As(III) band could be attributed to the fact that the complexes of As(III) are IR inactivated or weakly activated,[44] so that it is overlapped by the bands of As(V) complexes (Figure 3B). It is also possible that the adsorption of As(III) does not involve direct coordination through a As(III)−O−Fe bond.[43] In contrast, some other mechanisms, such as hydrogen bonding, could be involved in the adsorption of As(III) over MIL-100(Fe).[25] Under alkaline conditions, the surface of MIL-100(Fe) was capped by an −OH group,[45] which formed hydrogen bonding with H_3AsO_3 (Figure 3D).[25]

Since H_2O_2 may be produced due to the reactions between Fe^{2+}/Fe^{3+} and oxygen, Fenton-like reactions should happen to generate ·OH as follows[46]

$$Fe^{2+} + H_2O_2 \rightarrow Fe^{3+} + \cdot OH + OH^- \quad (6)$$

$$Fe^{3+} + H_2O_2 \rightarrow Fe^{2+} + \cdot O_2H + H^+ \quad (7)$$

It should be noted that $\cdot O_2H$ may be altered to $O_2^{\cdot-}$ at the experimental pH.[44] These radicals are strong and nonselective oxidant,[47] which are capable of oxidizing As(III) to As(V).[30,32]

To elucidate this mechanism, we verified the production of H_2O_2 through a colorimetric detection method.[48] In the presence of H_2O_2, the colorless $TiOSO_4$ solution would turn to be yellowish. By measuring the absorption intensity at 405 nm, the amount of H_2O_2 can be determined. As shown in Figure 4A, when 3 V of voltage was applied and air was bubbled into the system, H_2O_2 was produced at a rate of 0.061 mg/L·h. This result is reasonable because we also observed that the level of dissolved oxygen increased over time due to air bubbling (Figure S8). The produced H_2O_2 initiated the Fenton-like reactions in the presence of Fe^{2+}/Fe^{3+} and form ROS, such as ·OH, which was further confirmed using a fluorescence technique.[49] At specific time intervals, water samples were collected from the filter holder and then mixed with coumarin. As shown in Figure 4A, fluorescence peaks can be identified at 455 nm. These peaks are indexed to be the product of the reaction between coumarin and ·OH.[49] Even though it is difficult to quantify the amount of ·OH with this method, the evolution of the fluorescence spectra clearly indicate the continuous accumulation of ·OH near the MIL-100(Fe) filter. Production of ·OH was further confirmed using EPR spectroscopy with DMPO as spin trap.[50] As shown in Figure 4B, EPR analysis of DMPO-treated aqueous samples aliquoted from the filter resulted in the characteristic four-line 1:2:2:1 hyperfine splitting pattern ($A_H = A_N$ = 14.9 G) associated with the DMPO/·OH spin adduct, confirming the generation of ·OH. In contrast, no pattern was observed for the sample obtained at 0 h, suggesting the production of ·OH during the treatment process.

To further verify this mechanism, we conducted XPS characterization for the MIL-100(Fe) before and after the As removal. As shown in Figure 4C, the Fe 2p spectrum can be deconvoluted into two major peaks at 710.4 and 724.1 eV, corresponding to Fe $2p_{3/2}$ and $2p_{1/2}$, respectively. Meanwhile, we also observed two satellite peaks at 716.6 and 727.2 eV, which are similar to a previous study.[51] The peak of Fe $2p_{3/2}$ can be further deconvoluted into two peaks at 710.2 and 712.1 eV, suggesting the existence of both Fe^{2+} and Fe^{3+}.[52] These

DOI: 10.1021/acs.est.7b06212
Environ. Sci. Technol. 2018, 52, 4275−4284

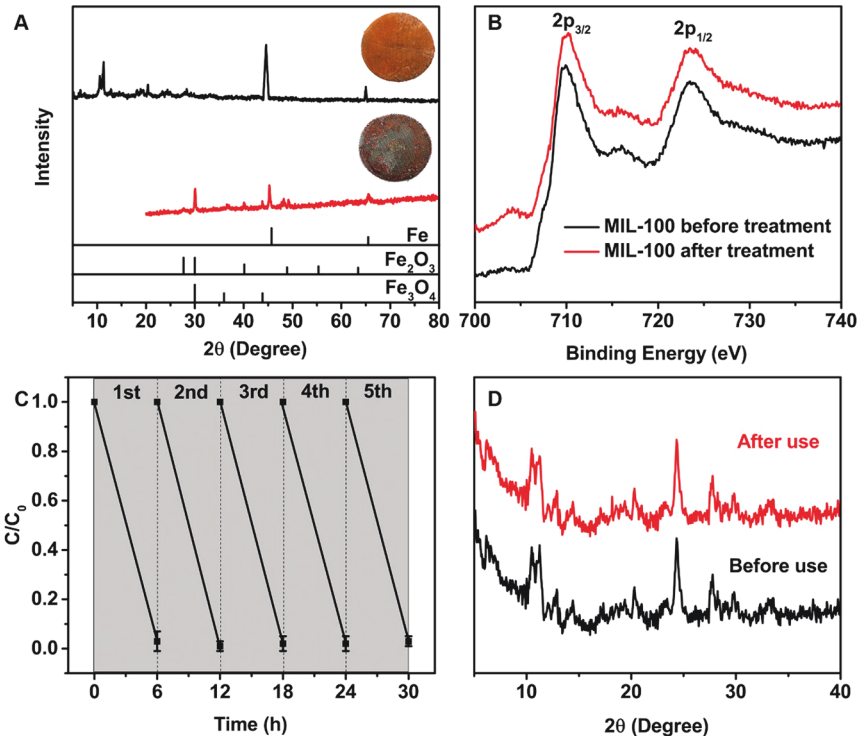

Figure 5. (A) XRD patterns of pristine iron mesh- (red) and MIL-100(Fe)-based (black) filters after the arsenic removal tests. (Insets) Corresponding digital images. (B) XPS spectra of Fe 2p from the MIL-100(Fe)-based filter before and after treatment. (C) Recycle performance of the As(III) removal over the MIL-100(Fe)-based filter, air bubbling, and 3 V of voltage were applied; no treatment of the filter was conducted between each cycle. (D) XRD patterns for the MIL-100(Fe) before and after recycle use.

coordinatively unsaturated iron sites are considered to be involved in the Fenton-like reaction to oxidize As(III) into As(V) since we observed the oxidation of As(III). As shown in the XPS spectrum of As 3d, three peaks, which correspond to As−O (43.6 eV), As^{3+} (44.5 eV), and As^{5+} (45.4 eV),[53] were observed (Figure 4D). Since the initial dose of arsenic was As(III), the presence of As(V) verified the oxidation from As(III) to As(V).

On the basis of the above analysis, we proposed a possible mechanism of the fast removal of As(III) over a MIL-100(Fe)-based filter: MIL-100(Fe) with a microporous structure and superior adsorption capacity adsorbs As(III) in a time-efficient manner and thus increased the concentration of As(III) near its surface significantly. On the other hand, the coordinatively unsaturated sites (Fe^{2+} and Fe^{3+}) within MIL-100(Fe) initiate the Fenton-like reactions in the presence of oxygen. Meanwhile, the increased As(III) concentration over MIL-100(Fe) accelerates its oxidation to As(V), which is more readily to be adsorbed. This mechanism is illustrated in Scheme 1. By applying certain voltages, the Fenton-like reactions are further accelerated due to the increased temperature, which is caused by the Joule heating effect.

3.4. Recycle Performance. As mentioned above, even pristine iron mesh shows certain adsorption capacity toward both As(III) and As(V). We found that after the arsenic removal tests, the pristine iron mesh was partially covered by corrosion (inset in Figure 5A). The XRD analysis confirms that, besides iron, Fe_3O_4 (PDF no. 74-1909) and Fe_2O_3 (PDF no. 24-0072) are also produced. Some other iron-bearing minerals were missing from the XRD pattern probably due to their low crystallinity. Meanwhile, the formation of $CaCO_3$ (PDF no. 29-305, all of the other peaks in Figure 5A) further implies that some complicated reactions may happen between iron mesh, dissolved oxygen, and the water components in the solution. Regarding the formation of iron oxides, the reactions between O_2 and Fe should play a major role. It has been recognized that, even under ambient conditions, Fe can react with pure water to produce iron oxides.[34] Since Fe_3O_4 has been reported to be of adsorption capacity toward arsenic,[31] we thus observed the removal of arsenic with pristine iron mesh.

For the MIL-100(Fe)-based filter, we observed no significant change of its outward after the arsenic removal tests. As shown in the inset of Figure 5A, the filter after the test also shows a color of orange, which is identical with the fresh filter (Figure 1G). Notably, only XRD peaks corresponding to MIL-100(Fe) and Fe can be found, indicating the structural stability of the MIL-100(Fe)-based filter, even in the presence of complicated water components (Figure 5A). The XPS spectra of Fe 2p from the MIL-100(Fe) also show the similar identity (Figure 5B), implying that oxidation status of Fe may remain constant before and after use. The full-scan XPS spectra of MIL-100(Fe) before and after use are also shown in Figure S9. All of the major peaks of MIL-100(Fe), including C 1s, O 1s, Fe 2p, and O KL1, were observed for the used samples, further indicating the strong structural integrity of MIL-100(Fe). Moreover, we also found the peaks corresponded to Na 1s and Cl 2s for the used MIL-100(Fe), which should be from the water components of synthetic groundwater. The SEM images of the MIL-100(Fe) filter after 5 cycle use (Figure S10) show little difference as compared to that of as-synthesized filter (Figure S1). This structural stability also suggests a possibly satisfactory recycle performance.

We also studied the recyclability of the MIL-100(Fe)-based filter to evaluate its potential for long-term use. The

DOI: 10.1021/acs.est.7b06212
Environ. Sci. Technol. 2018, 52, 4275−4284

performance of the MIL-100(Fe)-based filter for As(III) removal was recorded for five consecutive cycles. A voltage of 3 V and air bubbling were applied in this experiment. As shown in Figure 5C, no inactivation of the As(III) removal efficiency was observed at the end of the fifth cycle, suggesting a satisfactory recycle performance of the filter. We further measured the adsorption capacity of MIL-100(Fe)-based filter and found that its capacity for As(III) and As(V) was 35.2 and 19.2 mg/g, respectively. The total volume of synthetic Bangladesh groundwater that can be treated by the system was estimated to be 14.4−26.4 L depending on the species of As (see Supporting Information). Meanwhile, the adsorption of As(III) and As(V) was found to follow the Freundlich and Langmuir models, respectively (Figure S11). The demonstrated adsorption capacity is lower than some MOFs-based adsorbents (Table S2), probably due to (I) the low adsorption capacity of bulk iron mesh and (II) the negative effects of water components (especially Si and P) in the synthetic groundwater on the adsorption of As.[32]

Since the dosing amount of As is only 0.5 mg for each test, which is significantly lower than the adsorption capacity, we observed a stable performance of the filter. In addition, the leaked iron species in the treated water was determined to be 18.9 μg for each cycle, which only accounted for 0.5‰ of the MIL-100(Fe)-based filter (weight = 0.375 g). The little amount of leaked iron suggested a reasonable stability of the filter and was consistent with the absence of As−Fe-DOM complexes in the water (Figure S4). Considering the effects of Joule heating and complicated water components, the recycle performance of the MIL-100(Fe)-based filter is impressive. In the arsenic removal tests where water flows through the filter, the temperature of the filter surface is 27.0 °C when 3 V is applied. In the absence of water flow, the temperature of the filter surface rises to 73.2 °C. Both temperatures cannot destroy the structure of MIL-100(Fe) since it can maintain its stability up to 270 °C.[16] As a result, Joule heating due to relative low voltages shows no adverse effects on the recycle performance of the MIL-100(Fe)-based filter. Regarding the effect of complex water components, MIL-100(Fe) is one of the most stable MOFs and able to maintain its structural integrity over a wide range of pH.[45] The pH value of the synthetic Bangladesh groundwater is 8.57, which is not harsh for MIL-100(Fe). Meanwhile, MIL-100(Fe) also acts as a protective layer and thus benefits the stability of iron mesh underneath (Figure 5D) since we did not observe any disruption of the filter.

It is understandable that even though the performance of the MIL-100(Fe)-based filter does not degrade after 5 cycles, some arsenic is adsorbed. If the filter is used for a long enough time, the possible saturation of adsorption capacity should inactivate its performance. However, the satisfactory stability of the MIL-100(Fe)-based filter enables us to regenerating its removal capacity when its adsorption reaches its saturation. We used the mixture solution of NaOH (5 wt %) and NaCl (5 wt %) for the regeneration of the adsorption-saturated filter.[35,54] After being immersed in the regeneration solution at 80 °C for 3 h, the filter maintained a satisfactory adsorption capacity to As over four cycles (Table S3), suggesting the potential of the MIL-100(Fe)-based filter for long-term use.

In summary, we developed a MIL-100(Fe)-based filter for arsenic removal from groundwater. The filter serves as a dual-functional system for the oxidation of As(III) and the adsorption of the generated As(V). Complete removal of As(III) can be achieved within 6 h with the aid of oxygen and Joule heating. The satisfactory structural stability and recycle performances suggest the potential of the filter for the remediation of arsenic contamination in groundwater. It is believed that the removal efficiency of arsenic can be further improved by connecting several filters in tandem. Future studies should consider the effect of pH for potentially wider applications. Future efforts to study the oxidation kinetics of As(III) by dual-functional adsorbents (oxidation and adsorption) are also urgently necessary. We also expect that by varying metal meshes, different MOFs can be implanted and produce their corresponding filters with specific functionality, which may advance clean water technologies.

■ ASSOCIATED CONTENT

Supporting Information

The Supporting Information is available free of charge on the ACS Publications website at DOI: 10.1021/acs.est.7b06212.

Supplementary experimental details, discussion on the formation mechanism of MIL-100(Fe) on iron mesh, surface area of pristine iron mesh, and total volume of groundwater can be treated by single filter (PDF)

■ AUTHOR INFORMATION

Corresponding Author

*E-mail: wnwang@vcu.edu.

ORCID

Dawei Wang: 0000-0002-3341-3544
Heather R. Lucas: 0000-0003-1207-7550
Wei-Ning Wang: 0000-0002-1935-6301

Author Contributions

W.N.W. supervised the project. D.W. conducted materials synthesis, characterization, and sample analysis. S.E.G. conducted BET and XPS analysis. X.Y. and K.L. contributed to materials synthesis and sample analysis. D.R.H. and H.R.L. helped with EPR analysis. D.W. and W.N.W. wrote the paper, and all authors contributed to discussion.

Notes

The authors declare no competing financial interest.

■ ACKNOWLEDGMENTS

We acknowledge support from the American Chemical Society Petroleum Research Fund (57072-DNI10) and the National Science Foundation (CMMI-1727553). H.R.L. acknowledge, the National Institute on Aging (L-13046) for the EPR spectrometer and the Altria Group, Inc., for research fellowship support of D.R.H. (Altria graduate fellow).

■ REFERENCES

(1) Rodríguez-Lado, L.; Sun, G.; Berg, M.; Zhang, Q.; Xue, H.; Zheng, Q.; Johnson, C. A. Groundwater Arsenic Contamination Throughout China. *Science* **2013**, *341* (6148), 866−868.

(2) Berg, M.; Tran, H. C.; Nguyen, T. C.; Pham, H. V.; Schertenleib, R.; Giger, W. Arsenic Contamination of Groundwater and Drinking Water in Vietnam: A Human Health Threat. *Environ. Sci. Technol.* **2001**, *35* (13), 2621−2626.

(3) Arsenic in groundwater of the United States. https://water.usgs.gov/nawqa/trace/arsenic/ (June 30, 2017).

(4) Singh, R.; Singh, S.; Parihar, P.; Singh, V. P.; Prasad, S. M. Arsenic contamination, consequences and remediation techniques: A review. *Ecotoxicol. Environ. Saf.* **2015**, *112*, 247−270.

DOI: 10.1021/acs.est.7b06212
Environ. Sci. Technol. 2018, 52, 4275−4284

(5) Mohan, D.; Pittman, C. U., Jr Arsenic removal from water/wastewater using adsorbents—A critical review. *J. Hazard. Mater.* **2007**, *142* (1−2), 1−53.
(6) Dutta, P. K.; Pehkonen, S. O.; Sharma, V. K.; Ray, A. K. Photocatalytic Oxidation of Arsenic(III): Evidence of Hydroxyl Radicals. *Environ. Sci. Technol.* **2005**, *39* (6), 1827−1834.
(7) Leupin, O. X.; Hug, S. J. Oxidation and removal of arsenic (III) from aerated groundwater by filtration through sand and zero-valent iron. *Water Res.* **2005**, *39* (9), 1729−1740.
(8) Boccelli, D. L.; Small, M. J.; Dzombak, D. A. Enhanced Coagulation for Satisfying the Arsenic Maximum Contaminant Level under Variable and Uncertain Conditions. *Environ. Sci. Technol.* **2005**, *39* (17), 6501−6507.
(9) Han, B.; Runnells, T.; Zimbron, J.; Wickramasinghe, R. Arsenic removal from drinking water by flocculation and microfiltration. *Desalination* **2002**, *145* (1), 293−298.
(10) Fox, D. I.; Stebbins, D. M.; Alcantar, N. A. Combining Ferric Salt and Cactus Mucilage for Arsenic Removal from Water. *Environ. Sci. Technol.* **2016**, *50* (5), 2507−2513.
(11) Ratna Kumar, P.; Chaudhari, S.; Khilar, K. C.; Mahajan, S. P. Removal of arsenic from water by electrocoagulation. *Chemosphere* **2004**, *55* (9), 1245−1252.
(12) Si, Y.; Li, G.; Zhang, F. Energy-Efficient Oxidation and Removal of Arsenite from Groundwater Using Air-Cathode Iron Electrocoagulation. *Environ. Sci. Technol. Lett.* **2017**, *4* (2), 71−75.
(13) Tong, M.; Yuan, S.; Zhang, P.; Liao, P.; Alshawabkeh, A. N.; Xie, X.; Wang, Y. Electrochemically Induced Oxidative Precipitation of Fe(II) for As(III) Oxidation and Removal in Synthetic Groundwater. *Environ. Sci. Technol.* **2014**, *48* (9), 5145−5153.
(14) Zhang, G.; Liu, F.; Liu, H.; Qu, J.; Liu, R. Respective Role of Fe and Mn Oxide Contents for Arsenic Sorption in Iron and Manganese Binary Oxide: An X-ray Absorption Spectroscopy Investigation. *Environ. Sci. Technol.* **2014**, *48* (17), 10316−10322.
(15) Férey, G.; Mellot-Draznieks, C.; Serre, C.; Millange, F.; Dutour, J.; Surblé, S.; Margiolaki, I. A Chromium Terephthalate-Based Solid with Unusually Large Pore Volumes and Surface Area. *Science* **2005**, *309* (5743), 2040−2042.
(16) Horcajada, P.; Surble, S.; Serre, C.; Hong, D.-Y.; Seo, Y.-K.; Chang, J.-S.; Greneche, J.-M.; Margiolaki, I.; Ferey, G. Synthesis and catalytic properties of MIL-100(Fe), an iron(iii) carboxylate with large pores. *Chem. Commun.* **2007**, No. 27, 2820−2822.
(17) Tan, F.; Liu, M.; Li, K.; Wang, Y.; Wang, J.; Guo, X.; Zhang, G.; Song, C. Facile synthesis of size-controlled MIL-100(Fe) with excellent adsorption capacity for methylene blue. *Chem. Eng. J.* **2015**, *281*, 360−367.
(18) Li, S.; Chen, Y.; Pei, X.; Zhang, S.; Feng, X.; Zhou, J.; Wang, B. Water Purification: Adsorption over Metal-Organic Frameworks. *Chin. J. Chem.* **2016**, *34* (2), 175−185.
(19) Folens, K.; Leus, K.; Nicomel, N. R.; Meledina, M.; Turner, S.; Van Tendeloo, G.; Laing, G. D.; Van Der Voort, P. Fe_3O_4@MIL-101 − A Selective and Regenerable Adsorbent for the Removal of As Species from Water. *Eur. J. Inorg. Chem.* **2016**, *2016* (27), 4395−4401.
(20) Audu, C. O.; Nguyen, H. G. T.; Chang, C.-Y.; Katz, M. J.; Mao, L.; Farha, O. K.; Hupp, J. T.; Nguyen, S. T. The dual capture of AsV and AsIII by UiO-66 and analogues. *Chem. Sci.* **2016**, *7* (10), 6492−6498.
(21) Jian, M.; Wang, H.; Liu, R.; Qu, J.; Wang, H.; Zhang, X. Self-assembled one-dimensional MnO_2@zeolitic imidazolate framework-8 nanostructures for highly efficient arsenite removal. *Environ. Sci.: Nano* **2016**, *3* (5), 1186−1194.
(22) Li, J.; Wu, Y.-n.; Li, Z.; Zhang, B.; Zhu, M.; Hu, X.; Zhang, Y.; Li, F. Zeolitic Imidazolate Framework-8 with High Efficiency in Trace Arsenate Adsorption and Removal from Water. *J. Phys. Chem. C* **2014**, *118* (47), 27382−27387.
(23) Zhu, B.-J.; Yu, X.-Y.; Jia, Y.; Peng, F.-M.; Sun, B.; Zhang, M.-Y.; Luo, T.; Liu, J.-H.; Huang, X.-J. Iron and 1,3,5-Benzenetricarboxylic Metal−Organic Coordination Polymers Prepared by Solvothermal Method and Their Application in Efficient As(V) Removal from Aqueous Solutions. *J. Phys. Chem. C* **2012**, *116* (15), 8601−8607.
(24) Wang, C.; Liu, X.; Chen, J. P.; Li, K. Superior removal of arsenic from water with zirconium metal-organic framework UiO-66. *Sci. Rep.* **2015**, *5*, 16613.
(25) Yang, J.-C.; Yin, X.-B. $CoFe_2O_4$@MIL-100(Fe) hybrid magnetic nanoparticles exhibit fast and selective adsorption of arsenic with high adsorption capacity. *Sci. Rep.* **2017**, *7*, 40955.
(26) Yoon, J. W.; Seo, Y.-K.; Hwang, Y. K.; Chang, J.-S.; Leclerc, H.; Wuttke, S.; Bazin, P.; Vimont, A.; Daturi, M.; Bloch, E.; Llewellyn, P. L.; Serre, C.; Horcajada, P.; Grenèche, J.-M.; Rodrigues, A. E.; Férey, G. Controlled Reducibility of a Metal−Organic Framework with Coordinatively Unsaturated Sites for Preferential Gas Sorption. *Angew. Chem., Int. Ed.* **2010**, *49* (34), 5949−5952.
(27) Tareq, S. M.; Maruo, M.; Ohta, K. Characteristics and role of groundwater dissolved organic matter on arsenic mobilization and poisoning in Bangladesh. *Physics and Chemistry of the Earth, Parts A/B/C* **2013**, *58*−*60*, 77−84.
(28) Lowell, S.; Shields, J. E.; Thomas, M. A.; Thommes, M. *Characterization of Porous Solids and Powders: Surface Area, Pore Size and Density*; Springer: Netherlands, 2004; pp 12−13.
(29) Sindoro, M.; Yanai, N.; Jee, A.-Y.; Granick, S. Colloidal-Sized Metal−Organic Frameworks: Synthesis and Applications. *Acc. Chem. Res.* **2014**, *47* (2), 459−469.
(30) Hug, S. J.; Leupin, O. Iron-Catalyzed Oxidation of Arsenic(III) by Oxygen and by Hydrogen Peroxide: pH-Dependent Formation of Oxidants in the Fenton Reaction. *Environ. Sci. Technol.* **2003**, *37* (12), 2734−2742.
(31) Prucek, R.; Tuček, J.; Kolařík, J.; Filip, J.; Marušák, Z.; Sharma, V. K.; Zbořil, R. Ferrate(VI)-Induced Arsenite and Arsenate Removal by In Situ Structural Incorporation into Magnetic Iron(III) Oxide Nanoparticles. *Environ. Sci. Technol.* **2013**, *47* (7), 3283−3292.
(32) Roberts, L. C.; Hug, S. J.; Ruettimann, T.; Billah, M. M.; Khan, A. W.; Rahman, M. T. Arsenic Removal with Iron(II) and Iron(III) in Waters with High Silicate and Phosphate Concentrations. *Environ. Sci. Technol.* **2004**, *38* (1), 307−315.
(33) Mohebbi, H.; Li, C. Q. Experimental Investigation on Corrosion of Cast Iron Pipes. *Int. J. Corros.* **2011**, *2011*, 506501.
(34) Whitney, W. R. the Corrosion of Iron. *J. Am. Chem. Soc.* **1903**, *25* (4), 394−406.
(35) Zhang, X.; Wu, M.; Dong, H.; Li, H.; Pan, B.-C. Simultaneous Oxidation and Sequestration of As(III) from Water by Using Redox Polymer-based Fe(III) oxide Nanocomposite. *Environ. Sci. Technol.* **2017**, *51* (11), 6326−6334.
(36) Redman, A. D.; Macalady, D. L.; Ahmann, D. Natural Organic Matter Affects Arsenic Speciation and Sorption onto Hematite. *Environ. Sci. Technol.* **2002**, *36* (13), 2889−2896.
(37) Giasuddin, A. B. M.; Kanel, S. R.; Choi, H. Adsorption of Humic Acid onto Nanoscale Zerovalent Iron and Its Effect on Arsenic Removal. *Environ. Sci. Technol.* **2007**, *41* (6), 2022−2027.
(38) Du, J.; Jing, C.; Duan, J.; Zhang, Y.; Hu, S. Removal of arsenate with hydrous ferric oxide coprecipitation: Effect of humic acid. *J. Environ. Sci.* **2014**, *26* (2), 240−247.
(39) Zhang, W.; Li, Y.; Wang, C.; Wang, P.; Wang, Q.; Wang, D. Mechanisms of simultaneous hydrogen production and estrogenic activity removal from secondary effluent though solar photocatalysis. *Water Res.* **2013**, *47* (9), 3173−3182.
(40) Mladenov, N.; Zheng, Y.; Simone, B.; Bilinski, T. M.; McKnight, D. M.; Nemergut, D.; Radloff, K. A.; Rahman, M. M.; Ahmed, K. M. Dissolved Organic Matter Quality in a Shallow Aquifer of Bangladesh: Implications for Arsenic Mobility. *Environ. Sci. Technol.* **2015**, *49* (18), 10815−10824.
(41) Sharma, P.; Ofner, J.; Kappler, A. Formation of Binary and Ternary Colloids and Dissolved Complexes of Organic Matter, Fe and As. *Environ. Sci. Technol.* **2010**, *44* (12), 4479−4485.
(42) Liu, G.; Fernandez, A.; Cai, Y. Complexation of Arsenite with Humic Acid in the Presence of Ferric Iron. *Environ. Sci. Technol.* **2011**, *45* (8), 3210−3216.
(43) Goldberg, S.; Johnston, C. T. Mechanisms of Arsenic Adsorption on Amorphous Oxides Evaluated Using Macroscopic

DOI: 10.1021/acs.est.7b06212
Environ. Sci. Technol. 2018, 52, 4275−4284

Measurements, Vibrational Spectroscopy, and Surface Complexation Modeling. *J. Colloid Interface Sci.* **2001**, *234* (1), 204−216.
(44) Voegelin, A.; Hug, S. J. Catalyzed Oxidation of Arsenic(III) by Hydrogen Peroxide on the Surface of Ferrihydrite: An in Situ ATR-FTIR Study. *Environ. Sci. Technol.* **2003**, *37* (5), 972−978.
(45) Bellido, E.; Guillevic, M.; Hidalgo, T.; Santander-Ortega, M. J.; Serre, C.; Horcajada, P. Understanding the Colloidal Stability of the Mesoporous MIL-100(Fe) Nanoparticles in Physiological Media. *Langmuir* **2014**, *30* (20), 5911−5920.
(46) Fenton, H. J. H. LXXIII.-Oxidation of tartaric acid in presence of iron. *J. Chem. Soc., Trans.* **1894**, *65* (0), 899−910.
(47) Kim, D.-h.; Bokare, A. D.; Koo, M. s.; Choi, W. Heterogeneous Catalytic Oxidation of As(III) on Nonferrous Metal Oxides in the Presence of H_2O_2. *Environ. Sci. Technol.* **2015**, *49* (6), 3506−3513.
(48) Eisenberg, G. Colorimetric Determination of Hydrogen Peroxide. *Ind. Eng. Chem., Anal. Ed.* **1943**, *15* (5), 327−328.
(49) Ishibashi, K.-i.; Fujishima, A.; Watanabe, T.; Hashimoto, K. Detection of active oxidative species in TiO_2 photocatalysis using the fluorescence technique. *Electrochem. Commun.* **2000**, *2* (3), 207−210.
(50) Bosnjakovic, A.; Schlick, S. Nafion Perfluorinated Membranes Treated in Fenton Media: Radical Species Detected by ESR Spectroscopy. *J. Phys. Chem. B* **2004**, *108* (14), 4332−4337.
(51) Zhang, F.; Shi, J.; Jin, Y.; Fu, Y.; Zhong, Y.; Zhu, W. Facile synthesis of MIL-100(Fe) under HF-free conditions and its application in the acetalization of aldehydes with diols. *Chem. Eng. J.* **2015**, *259*, 183−190.
(52) Li, P.; Jiang, E. Y.; Bai, H. L. Fabrication of ultrathin epitaxial γ-Fe_2O_3 films by reactive sputtering. *J. Phys. D: Appl. Phys.* **2011**, *44* (7), 075003.
(53) Vadahanambi, S.; Lee, S.-H.; Kim, W.-J.; Oh, I.-K. Arsenic Removal from Contaminated Water Using Three-Dimensional Graphene-Carbon Nanotube-Iron Oxide Nanostructures. *Environ. Sci. Technol.* **2013**, *47* (18), 10510−10517.
(54) Chaudhary, B. K.; Farrell, J. Understanding Regeneration of Arsenate-Loaded Ferric Hydroxide-Based Adsorbents. *Environ. Eng. Sci.* **2015**, *32* (4), 353−360.

DOI: 10.1021/acs.est.7b06212
Environ. Sci. Technol. 2018, 52, 4275−4284

Supporting Information for

Iron Mesh-Based Metal Organic Framework Filter for Efficient Arsenic Removal

Dawei Wang[†], Stanley E. Gilliland III[¶], Xinbei Yi[†], Kayla Logan[†], Denver R. Heitger[⊥], Heather R. Lucas[⊥], and Wei-Ning Wang[†,*]

[†]Department of Mechanical & Nuclear Engineering, Virginia Commonwealth University, Richmond, Virginia 23219, United States

[¶]Department of Chemical and Life Science Engineering, Virginia Commonwealth University, Richmond, VA 23219, United States

[⊥]Department of Chemistry, Virginia Commonwealth University, Richmond, VA 23284, United States

*Corresponding Author: E-mail: wnwang@vcu.edu

Number of pages: 14

Number of figures: 11

Number of tables: 3

Supplementary Characterization and Measurement Details

The crystal phase identification was obtained using a PANalytical X'Pert Pro MPD X-ray diffractometer equipped with a Cu-Kα radiation source (λ = 1.5401 Å). XRD patterns were collected at 40 kV and 45 mA. Brunauer-Emmett-Teller (BET) surface area was analyzed by an accelerated surface area and porosimetry system (ASAP 2020, Micrometirics) at 77 K. Optical images were obtained with an optical microscopy (Scope.A1, Zeiss). The morphology and size of the samples were analyzed with a Hitachi Su-70 field emission scanning electron microscope (FE-SEM). The transmission electron microscopy (TEM) images were obtained by using a JEOL JEM-1230 microscope with an acceleration voltage of 100 kV. To prepare samples for TEM characterization, MIL-100(Fe) on iron mesh was scratched off from the mesh and dispersed in EtOH. The suspension was drop-casted on copper grids for TEM imaging. The concentrations of As was determined by an inductively coupled plasma mass spectrometry (ICP-MS, Agilent 7700 series, detection limit is 11.9 ppt). To prepare for ICP-MS test, the collected water samples were diluted with HNO_3 solution to make 2% HNO_3 solution. Argon with ultrahigh purity (>99.99%) was used as carrier gas with a flow rate of 1.05 L/min. H_2O_2 was measured with an UV-visible spectrometer (Thermo Scientific Evolution 220) by determining the absorption intensity at 405 nm.[1] For the colorimetric detection of H_2O_2, water samples (1 mL) was mixed the $TiOSiO_4$ solution (1 mL) for UV-vis analysis. Fluorescence spectra were recorded with a fluorosepctrometer (PTI QuantaMaster 400, Horiba). The concentration of coumarin was 10^{-3} M, and the excitation wavelength was 350 nm. For the fluorescent detection

of hydroxyl radicals, water samples (1 mL) was mixed the coumarin solution (0.2 mL). IR spectra of solution were collected by injected solution (10 μL) onto the crystal of FTIR. X-ray photoelectron spectroscopy (XPS, Thermofisher ESCAlab 250) was used to determine the valance state of the produced As on the filter. The DO concentration was monitored using a Dissolved oxygen meter (ExStik II). The fluorescence EMMs was obtained using fluorescence spectrometer according to a previous study.[2] Electron paramagnetic resonance (EPR) spectroscopy (X-band Bruker EMX 6/1 spectrometer) analysis with 5,5-dimethyl-1-pyrroline-N-oxide (DMPO, from Dojindo Molecular Technologies, Inc.) was conducted to confirm the production of hydroxyl radicals. For EPR analysis, a water sample (after 2h treatment by the MIL-100(Fe) filter) was collected and transported on ice to the Lucas lab. The sample aliquot was mixed with an aqueous 5,5-dimethyl-1-pyrroline-*N*-oxide (DMPO). EPR parameters were as follows: microwave frequency = 9.86 GHz, microwave power = 0.687 mW, modulation amplitude = 1 G, modulation frequency = 100 KHz, receiver gain = 1000, center field = 3500 G, sweep width = 100 G, resolution = 1024 points, # of scans = 8, time constant = 0.64 ms, conversion time = 10.24 ms, sweep time = 10.486 s. Temperature of the filter was measured using a thermometer (HH308, OMEGAETTE).

Supplementary Discussion

The formation mechanism of MIL-100(Fe) on iron mesh

In a typical synthesis of MOF, metal salts, organic linkers, and solvent are mixed and allowed to react at certain conditions (usually elevated temperature and pressure). At early stage of reaction, metal ions coordinate with organic linker to produce nuclei, and followed by growth process.[3] It has been reported that when the source of metal alternated to metal oxides, mechanism changes slightly: The first step is the dissolution of metal ions due to the etching of metal oxides.[4] Our recent study also confirmed this mechanism.[5] The dissolved metal ions then react with linker and undergo a nucleation and growth processes. We hypothesize that the above mechanism also works for metals since the aqueous solution of trimesic acid has a pH lower than 7, thus being able to etch iron mesh and release iron ions.

Surface area of pristine iron mesh

The area of the iron wire is

$$S = \pi dh \qquad \text{(S1)}$$

where d is the diameter and h is the length of iron wire.

The mass of the iron wire is

$$m = V\rho = \frac{1}{4}\pi d^2 h\rho \qquad \text{(S2)}$$

where V is the volume and ρ is the density of iron wire. Thus, the surface area of the iron wire is

$$A_s = \frac{S}{m} = \frac{4}{d\rho} = \frac{4}{200(\mu\text{m})\times 7.84\text{g/cm}^2} \approx 0.25\ \text{m}^2/\text{g} \qquad \text{(S3)}$$

Total volume of groundwater can be treated by single filter

The adsorption capacity of single filter was estimated to be 13.2 mg (= 35.2 mg/g × 0.375 g) for As(III) and 7.2 mg (= 19.2 mg/g × 0.375 g) for As(V), respectively. The arsenic concentration of synthetic groundwater was 0.5 mg/L, if the arsenic is all As(III), the total volume of groundwater can be treated is 26.4 L. And if the arsenic is all As(V), the total volume of groundwater can be treated is 14.4 L.

Supplementary Tables

Table S1. Experimental and calculated parameters

Dosed As	Adsorbents	Air bubbling	Voltage (V)	C_e (μg/L)	Removal efficiency (Total As, %)
III	Pristine iron	No	0	454.7	9.1
V	Pristine iron	No	0	420.05	16.0
III	MIL-100(Fe)	No	0	68.5	86.3
V	MIL-100(Fe)	No	0	Not detectable	100
III	Pristine iron	Yes	0	454.35	9.2
III	MIL-100(Fe)	Yes	0	42.6	91.5
III	MIL-100(Fe)	Yes	1.5	2.65	94.7
III	MIL-100(Fe)	No	1.5	80.0	83.9
III	MIL-100(Fe)	Yes	3	Not detectable	100
III	MIL-100(Fe)	No	3	105.5	78.9
III	MIL-100(Fe)	Yes	4.5	45.65	90.9
III	MIL-100(Fe)	No	4.5	132.3	73.4

Table S2. Comparison of adsorption capacity with previous MOFs-based adsorbents

Adsorbents	Adsorption capacity to As (III) (unit: mg/g)	Adsorption capacity to As (V) (unit: mg/g)	Form	Reference
UIO-66	40	90	powder	6
Fe-BTC	Not available	12	powder	7
ZIF-8	Not available	76.5	powder	8
MnO_2@ZIF-8	140.27	Not available	powder	9
UIO-66	Not available	303.3	powder	10
$CoFe_2O_4$@MIL-100(Fe)	143.6	114.8	powder	11
Fe mesh@MIL-100(Fe)	35.2	19.2	filter	This study

Table S3. Cyclic performance of the filter with regeneration

Cycles	As (III) capacity (mg/g)	As (V) capacity (mg/g)
1	35.2	19.2
2	34.8	18.4
3	34.6	18.6
4	34.3	18.2

Supplementary Figures

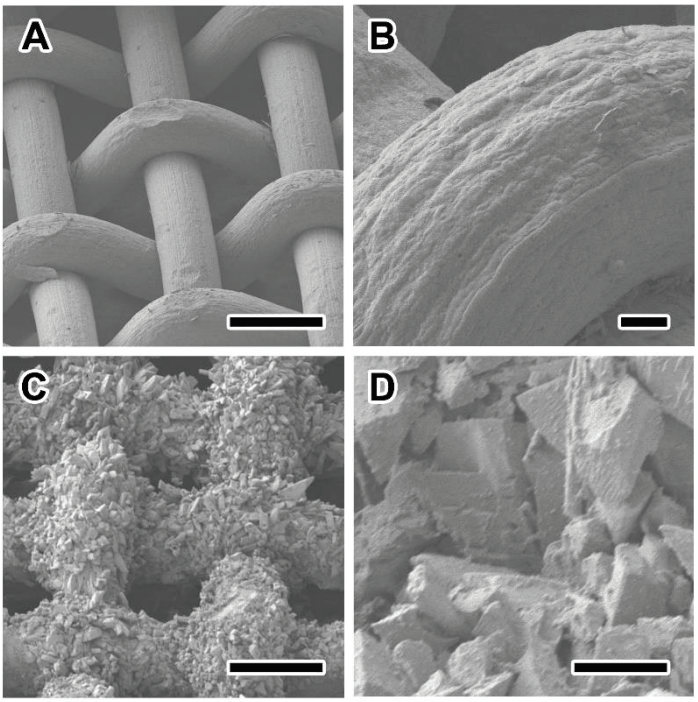

Figure S1. SEM images of (A and B) pristine iron mesh and (C and D) as-synthesized MIL-100(Fe) filter. Scale bars in A, B, C, and D represent 250 μm, 50 μm, 250 μm, and 50 μm, respectively.

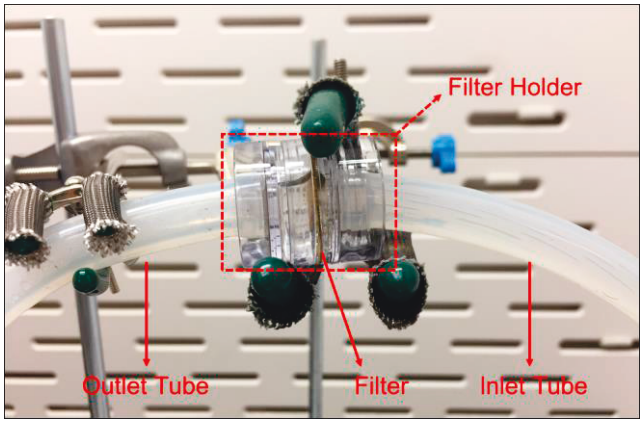

Figure S2. The digital images of the set-up for the filters.

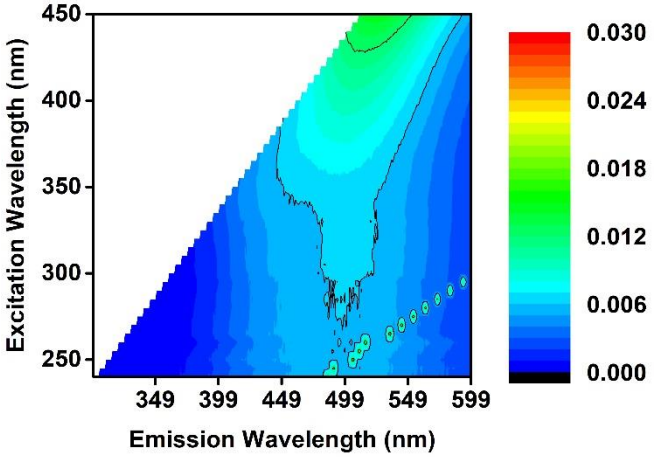

Figure S3. EEM of water (spiked with HA) treated by the MIL-100(Fe) filter without voltage applying. The matrices were similar with that of the fresh synthetic groundwater, suggesting no decomposition of HA under this condition. This result also implies the decomposition of HA (Figure 2C and 2D) can be ascribed to the redox reactions in the system.

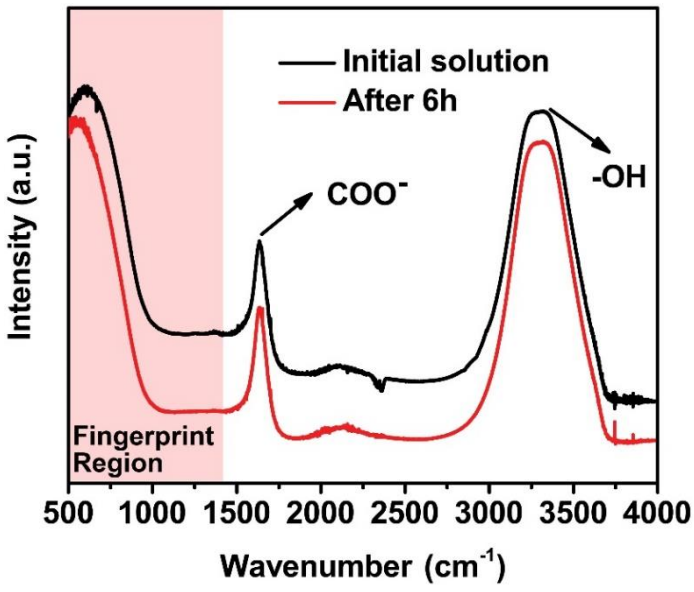

Figure S4. The FTIR spectra of the solution before and after 6-h filtration. The sharp peak at ~1600 cm^{-1} represent asymmetric and symmetric vibrations for COO^- of DOM. The As-Fe-DOM complexes should exhibit peaks ranged from 1400 to 2000 cm^{-1}.[12]

The absence of new peaks for the complexes is possibly due to the high stability of MIL-100(Fe) filter since the complexes of As-Fe-DOM is easily formed in the absence of sufficient Fe.[13] Fingerprint region is ranged from 500-1400 cm^{-1}. This region is a complex area showing many bands, such as C-C, C-O, and C-N.

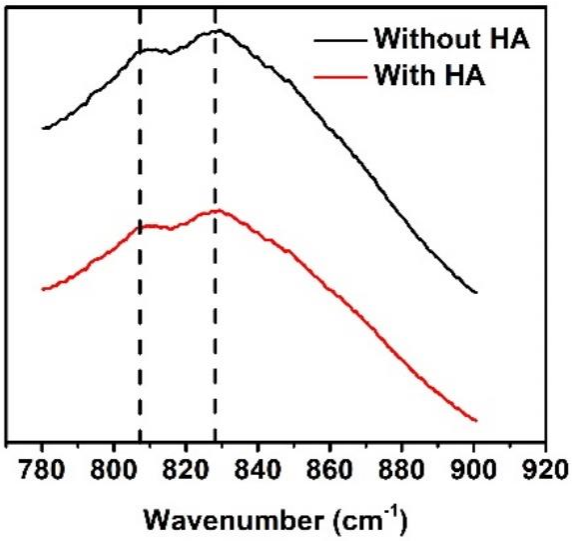

Figure S5. FTIR spectra of the MIL-100(Fe) filter after use in the synthetic groundwater with and without humic acid. No shift was observed, implying that there was no As-DOM forming on the surface of MIL-100(Fe) filter.[14]

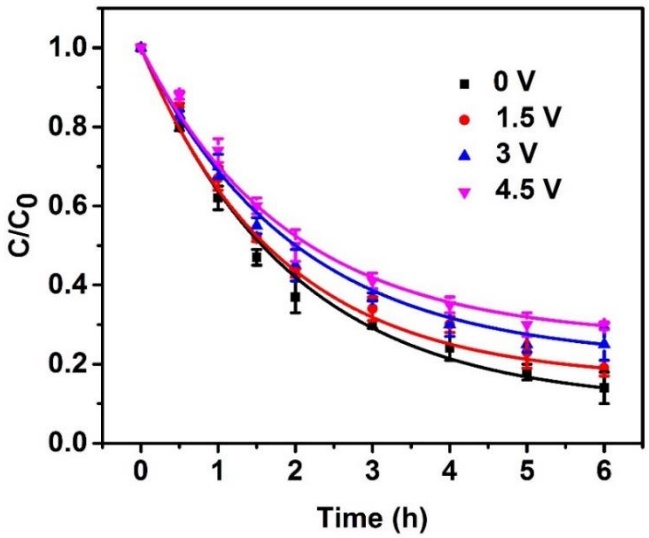

Figure S6. The effect of solo Joule heating on the removal efficiency of As (III).

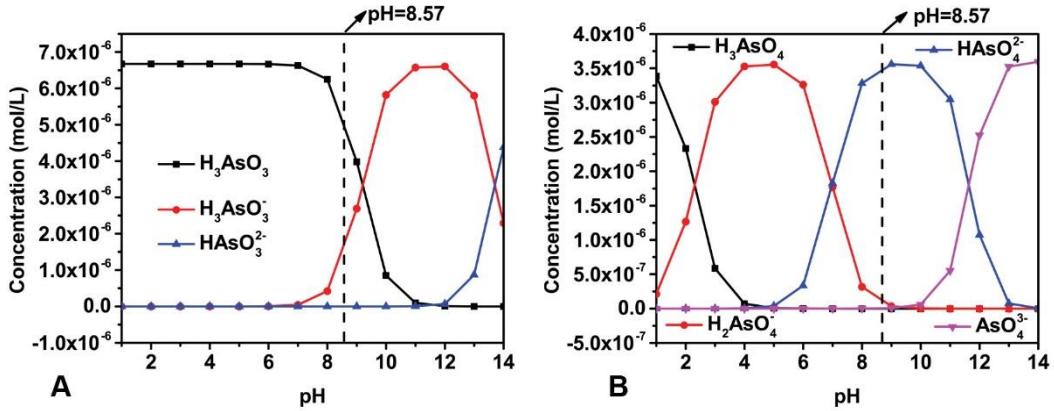

Figure S7. Distribution of arsenic species in water under different pH values: (A) is for As(III) and (B) is for As (V).

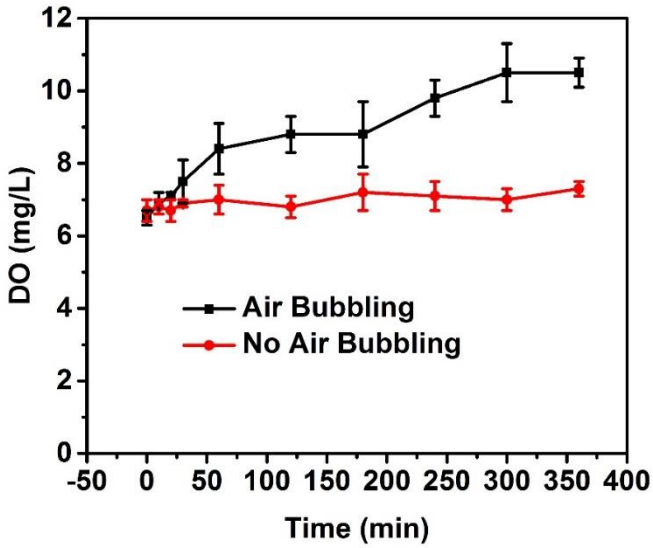

Figure S8. Dissolved oxygen concentrations changed over time.

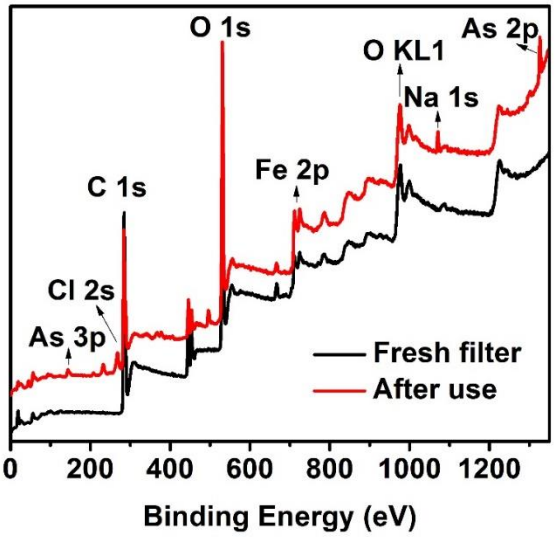

Figure S9. XPS spectra of fresh MIL-100 (Fe) and used one.

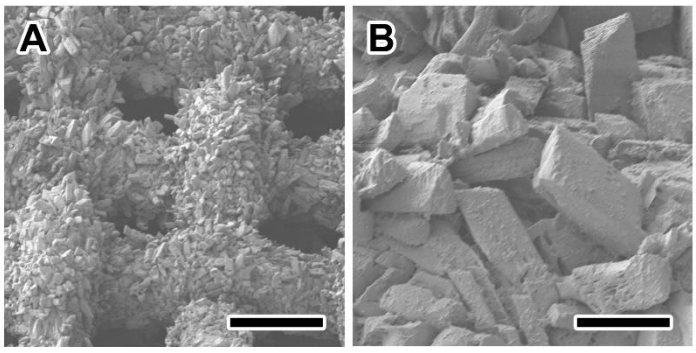

Figure S10. SEM images of MIL-100(Fe) filter after 5 cycle use. Scale bars in A and B represent 250 μm, and 50 μm, respectively.

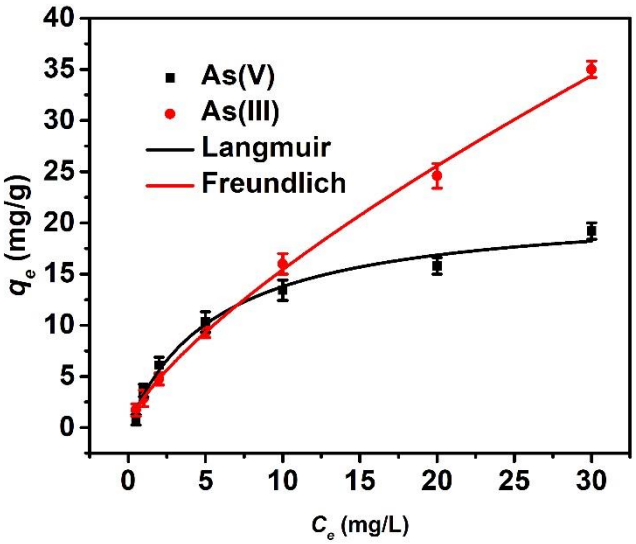

	k_F (mg/g)	n	k_L (mg/L)	q_{max} (mg/g)	R^2
As(III)	2.88	1.37		35.2	0.97
As(V)			0.17	19.2	0.98

Figure S11. Adsorption isotherms of As on the MIL-100(Fe) filter at room temperature. The Langmuir (Equation S1) and Freundlich (Equation S2) models were used to fit the isotherms.

$$\frac{C_e}{q_e} = \frac{C_e}{q_{max}} + \frac{1}{k_L q_{max}} \qquad \text{(S4)}$$

$$q_e = k_F C_e^{\frac{1}{n}} \qquad \text{(S5)}$$

where q_e (mg/g) is the As adsorbed on the filter at equilibrium, C_e is the equilibrium As concentration (mg/L), k_L is the constant of the Langmuir model, k_F and n are the constants of the Freundlich model.

Supplementary References

1. Eisenberg, G., Colorimetric Determination of Hydrogen Peroxide. *Ind. Eng. Chem. Anal. Ed.* **1943,** *15*, (5), 327-328.

2. Murphy, K. R.; Butler, K. D.; Spencer, R. G. M.; Stedmon, C. A.; Boehme, J. R.; Aiken, G. R., Measurement of Dissolved Organic Matter Fluorescence in Aquatic Environments: An Interlaboratory Comparison. *Environ. Sci. Technol.* **2010,** *44*, (24), 9405-9412.

3. Sindoro, M.; Yanai, N.; Jee, A.-Y.; Granick, S., Colloidal-Sized Metal–Organic Frameworks: Synthesis and Applications. *Acc. Chem. Res.* **2014,** *47*, (2), 459-469.

4. Zhan, W.-w.; Kuang, Q.; Zhou, J.-z.; Kong, X.-j.; Xie, Z.-x.; Zheng, L.-s., Semiconductor@Metal–Organic Framework Core–Shell Heterostructures: A Case of ZnO@ZIF-8 Nanorods with Selective Photoelectrochemical Response. *J. Am. Chem. Soc.* **2013,** *135*, (5), 1926-1933.

5. Wang, D.; Li, Z.; Zhou, J.; Fang, H.; He, X.; Jena, P.; Zeng, J.-B.; Wang, W.-N., Simultaneous Detection and Removal of Formaldehyde at Room Temperature: Janus Au@ZnO@ZIF-8 Nanoparticles. *Nano-Micro Lett.* **2018,** *10*, (1), 4.

6. Audu, C. O.; Nguyen, H. G. T.; Chang, C.-Y.; Katz, M. J.; Mao, L.; Farha, O. K.; Hupp, J. T.; Nguyen, S. T., The dual capture of AsV and AsIII by UiO-66 and analogues. *Chem. Sci.* **2016,** *7*, (10), 6492-6498.

7. Zhu, B.-J.; Yu, X.-Y.; Jia, Y.; Peng, F.-M.; Sun, B.; Zhang, M.-Y.; Luo, T.; Liu, J.-H.; Huang, X.-J., Iron and 1,3,5-Benzenetricarboxylic Metal–Organic Coordination Polymers Prepared by Solvothermal Method and Their Application in Efficient As(V) Removal from Aqueous Solutions. *J. Phys. Chem. C* **2012,** *116*, (15), 8601-8607.

8. Li, J.; Wu, Y.-n.; Li, Z.; Zhang, B.; Zhu, M.; Hu, X.; Zhang, Y.; Li, F., Zeolitic Imidazolate Framework-8 with High Efficiency in Trace Arsenate Adsorption and Removal from Water. *J. Phys. Chem. C* **2014,** *118*, (47), 27382-27387.

9. Jian, M.; Wang, H.; Liu, R.; Qu, J.; Wang, H.; Zhang, X., Self-assembled one-dimensional MnO2@zeolitic imidazolate framework-8 nanostructures for highly efficient arsenite removal. *Environ. Sci. Nano.***2016,** *3*, (5), 1186-1194.

10. Wang, C.; Liu, X.; Chen, J. P.; Li, K., Superior removal of arsenic from water with zirconium metal-organic framework UiO-66. *Sci. Rep.* **2015,** *5*, 16613.

11. Yang, J.-C.; Yin, X.-B., CoFe2O4@MIL-100(Fe) hybrid magnetic nanoparticles exhibit fast and selective adsorption of arsenic with high adsorption capacity. *Sci. Rep.* **2017,** *7*, 40955.

12. Sharma, P.; Ofner, J.; Kappler, A., Formation of Binary and Ternary Colloids and Dissolved Complexes of Organic Matter, Fe and As. *Environ. Sci. Technol.* **2010,** *44*, (12), 4479-4485.

13. Mladenov, N.; Zheng, Y.; Simone, B.; Bilinski, T. M.; McKnight, D. M.; Nemergut, D.; Radloff, K. A.; Rahman, M. M.; Ahmed, K. M., Dissolved Organic Matter Quality in a Shallow Aquifer of Bangladesh: Implications for Arsenic Mobility. *Environ. Sci. Technol.* **2015,** *49*, (18), 10815-10824.

14. Du, J.; Jing, C.; Duan, J.; Zhang, Y.; Hu, S., Removal of arsenate with hydrous ferric oxide coprecipitation: Effect of humic acid. *J. Environ. Sci.* **2014,** *26*, (2), 240-247.